



LUND UNIVERSITY

Two-dimensional OH-thermometry in reacting flows using photofragmentation laser-induced fluorescence

Malmqvist, Elin; Jonsson, Malin; Larsson, Kajsa; Aldén, Marcus; Bood, Joakim

Published in:
Combustion and Flame

DOI:
[10.1016/j.combustflame.2016.05.002](https://doi.org/10.1016/j.combustflame.2016.05.002)

2016

Document Version:
Peer reviewed version (aka post-print)

[Link to publication](#)

Citation for published version (APA):
Malmqvist, E., Jonsson, M., Larsson, K., Aldén, M., & Bood, J. (2016). Two-dimensional OH-thermometry in reacting flows using photofragmentation laser-induced fluorescence. *Combustion and Flame*, 169, 297-306. <https://doi.org/10.1016/j.combustflame.2016.05.002>

Total number of authors:
5

Creative Commons License:
CC BY-NC-ND

General rights

Unless other specific re-use rights are stated the following general rights apply:
Copyright and moral rights for the publications made accessible in the public portal are retained by the authors and/or other copyright owners and it is a condition of accessing publications that users recognise and abide by the legal requirements associated with these rights.

- Users may download and print one copy of any publication from the public portal for the purpose of private study or research.
- You may not further distribute the material or use it for any profit-making activity or commercial gain
- You may freely distribute the URL identifying the publication in the public portal

Read more about Creative commons licenses: <https://creativecommons.org/licenses/>

Take down policy

If you believe that this document breaches copyright please contact us providing details, and we will remove access to the work immediately and investigate your claim.

LUND UNIVERSITY

PO Box 117
221 00 Lund
+46 46-222 00 00

Two-dimensional OH-thermometry in reacting flows using photofragmentation laser-induced fluorescence

Elin Malmqvist*, Malin Jonsson, Kajsa Larsson, Marcus Aldén, Joakim Bood

Division of Combustion Physics, Department of Physics

Lund University, Box 118, 221 00 Lund, Sweden

*Corresponding Author: Elin Malmqvist

Email: elin.malmqvist@forbrf.lth.se

Phone: +46 46 222 33 25

Manuscript accepted for publication in Combustion and Flame 2016

Keywords: Thermometry, photofragmentation, laser-induced fluorescence, hydroxyl radical, imaging, HCCI engine, reacting flows

Abstract

In the present work, the possibility of using photofragmentation laser-induced fluorescence (PFLIF) for thermometry in different reacting flows is investigated. Hydroxyl (OH) fragments are created by UV-laser (266 nm) fragmentation of hydrogen peroxides (H_2O_2 and HO_2), whereupon the fluorescence, induced while scanning the wavelength of a second laser across the $\text{A}^2\Sigma^+(\text{v}=1) - \text{X}^2\Pi(\text{v}=0)$ absorption band (around 282 nm) of the generated OH fragments, is collected and detected. The temperature is determined by fitting simulated OH-excitation spectra of different temperatures to the experimentally recorded spectrum. In combustion, hydrogen peroxides are intermediate species formed during the low-temperature oxidation of the fuel, and hence they are present in a region covering a wide temperature span, ranging from unburnt to burnt gas temperatures. Thus, LIF of OH photofragments stemming from hydrogen peroxides allows for thermometry covering a wider temperature range than LIF of naturally present OH radicals. There is another important advantage of the concept in that the temperature sensitivity of OH excitation spectra is greater at lower temperatures. The method is demonstrated for two-dimensional (2-D) thermometry in three different measurement situations, namely a free flow of vaporized H_2O_2 at room temperature, a preheated mixture of $\text{CH}_4/\text{N}_2/\text{O}_2/\text{O}_3$ at intermediate temperatures (300 - 600 K), where the OH fragments stem from photodissociation of O_3 followed by chemical reactions, and in an optical homogeneous charge compression ignition (HCCI) engine prior to ignition, i.e. at elevated pressures and temperatures. It is found that the technique performs well in all three cases, with measured temperatures in good agreement with thermocouple readings, for the two first cases, and with temperatures calculated based on the ideal gas law using measured pressure traces as input for the engine measurements. The quantitative 2-D temperature images acquired in the engine experiments reveal inhomogeneous temperature distributions, clearly illustrating the capacity of the technique to yield crucial experimental input to engine modelers and designers. The

accuracy of the technique in the temperature range 300-600 K is lower than 23 K. For the room temperature case the precision is 4.3%, corresponding to 12 K.

1. Introduction

Combustion is a major source of energy production in our society, and it is likely to remain so in the foreseeable future. It involves complex processes characterized by complicated chemistry, typically involving hundreds of reactions and species, often taking place in a turbulent flow field. The chemical reaction rates, and therefore also chemical kinetics, are highly dependent on the surrounding temperature [1]. Temperature is thus one of the key factors determining the properties of the combustion process, such as pollution formation, particle formation, energy release rates, energy transfer and the overall combustion efficiency [2]. The ability to measure temperatures in different combustion systems is particularly crucial for validation of theoretical and numerical combustion models. The need for better and more accurate thermometry is therefore a major driving force in the development of new diagnostic techniques and concepts.

A number of different optical and laser-based diagnostic techniques have been developed during the last decades, and several of them are available for temperature measurements in different combustion environments. For point measurements, coherent anti-Stokes Raman spectroscopy (CARS) is often the most reliable technique, due to its superior signal to interference ratio, high precision, and high accuracy [3]. Recently, Bohlin et al. demonstrated two-dimensional (2-D) CARS for measurement of flame temperatures [4]. However, being based on advanced laser systems (fs and ps lasers), typically requiring stable and well controlled ambient conditions, its applicability under harsh conditions, such as those prevailing in a combustion engine laboratory, has yet to be investigated. In combustion, Rayleigh scattering has been used extensively for thermometry, since 2-D information may easily be acquired, and the data evaluation is relatively straightforward [5]. The signal levels in Rayleigh scattering are

usually relatively weak and the technique is limited to non-sooty environments. In addition, significant uncertainty due to the lack of effective Rayleigh cross sections is common, as the chemical composition often is unknown. Two-line atomic fluorescence (TLAF) is a method that allows single-shot 2-D thermometry by sensing the relative population of two atomic energy states and deducing the gas temperature from the Boltzmann distribution [6]. However, in order to capture a broad temperature interval and obtain strong signals, the technique requires seeding of a fluorescent, non-reacting atomic species, such as sodium, indium or gallium [6], which might not always be possible. This requirement may limit the practical utility of the technique [7]. Due to its high sensitivity and selectivity, as well as imaging capacity, laser-induced fluorescence (LIF) has been widely used for 2-D visualization of minor-species concentrations in combustion [8, 9]. Laser-induced fluorescence can also be utilized for thermometry via excitation spectra, 2-line excitation, or thermally assisted LIF [5, 10].

In combustion chemistry, the hydroxyl radical (OH) is an important species since it plays a vital role in the oxidation process of hydrocarbon fuels. It has been extensively studied with LIF in different combustion environments since the transition between the electronic ground state ($X^2\Pi$) and the first excited state ($A^2\Sigma^+$) is easily accessible by tunable dye lasers or optical parametric oscillators (OPOs) [10]. The hydroxyl radical is present in the reaction and product zones, but absent in the preheat zone, and its spatial derivative can thus be used as a marker for the flame front.

Thermometry based on OH has been realized through several different approaches, which often offer the possibility to measure temperature and OH concentration simultaneously. In an early study by Broida temperature was measured in a methane/air flame by analyzing the OH chemiluminescence and absorption spectra [11]. Line-of-sight techniques such as chemiluminescence and absorption, however, have the disadvantage that they require constant temperature throughout the entire probe volume to obtain the correct temperature. Methods

based on OH-LIF typically provide high spatial resolution, thereby avoiding the problem with non-thermal spectra, and thus providing higher accuracy. Temperature may be extracted by sensing the population on a multitude of rotational levels, i.e. by recording and analyzing an excitation spectrum [12-17] or by probing the populations on only two rotational states, whose ratio is strongly temperature dependent, which also allows single-shot measurement [18-23]. However, with both these approaches the gas temperature can only be measured where OH radicals are present.

The aim of the present study is a proof-of-concept demonstration of thermometry based on OH photofragments, which allows for thermometry in a temperature regime where natural OH is not present, and that the OH photofragment thermometry also represents an advantage since the temperature sensitivity of the OH rotational population distribution is greater at lower temperatures. The method, which allows two-dimensional temperature imaging, utilizes the temperature-dependent rotational population distribution of natural OH radicals as well as OH photofragments, which are created from a parent species via laser photolysis; a technique called photofragmentation laser-induced fluorescence (PFLIF). Photofragmentation laser-induced fluorescence, originally developed by Rodgers et al. [23], has in recent years been used for indirect visualization of hydrogen peroxides, through imaging of the OH photofragments with LIF, with applications in free gaseous flows [24, 25] and engines [26, 27]. In the present work OH fragments are produced through UV photolysis, either by direct dissociation of hydrogen peroxides or via dissociation of O_3 , forming O atoms that produce OH upon reaction with mainly CH_4 . The OH fragments are probed by a dye laser, whose wavelength is scanned across the $A^2\Sigma^+(v=1) \leftarrow X^2\Pi(v=0)$ absorption band while monitoring the fluorescence emitted in the $A^2\Sigma^+(v=0) \rightarrow X^2\Pi(v=0)$ band, which results in an OH excitation spectrum, whereupon the gas temperature is determined by a least-square fit to a library of excitation spectra calculated for different temperatures.

The measurement concept is demonstrated in a free flow containing H_2O_2 vapor, a heated gas mixture containing $\text{CH}_4/\text{N}_2/\text{O}_2/\text{O}_3$, and a homogeneous charge compression ignition (HCCI) engine. In the first two experiments the temperature is stable over time, which justifies the use of excitation scans. In the engine experiment, it might appear misbegotten to use excitation scan, which took about three minutes to record, as cycle-to-cycle variations could potentially distort the shape of the spectrum, making the method unreliable. Although the authors do not recommend excitation scan for engine thermometry in general, the fact that the measured spectra agree well with calculated spectra shows that experimental data are good enough to conceptually prove that thermometry based on OH fragments is feasible in an HCCI engine. In addition, previous thermometry in a spark-ignition engine, using rotational CARS, shows that cycle-to-cycle variations are minor prior to ignition [28]. Although the engines are different, the CARS study gives an indication that cycle-to-cycle variations might not be a major issue in our experiments, which were also carried out prior to ignition.

The following section outlines the OH-thermometry concept and the evaluation method. Then the experimental details of the three different measurement systems are described, before presenting and discussing the results. The paper ends with a section summarizing the conclusions drawn.

2. OH-thermometry concept

As mentioned in the introduction, the temperature is determined by fitting simulated OH excitation spectra to the experimental spectra. In an excitation spectrum the population on a number of rotational levels in a lower state, here the electronic ground state of OH ($X^2\Pi$), is probed through excitation to an upper electronic state, here $A^2\Sigma^+$, from which fluorescence is emitted and detected. The fluorescence signal intensity corresponding to each individual absorption transition is a measure of the population on the associated rotational level, which is temperature dependent. Given that the OH radicals are in thermal equilibrium, the shape of the

recorded spectrum reflects the temperature. Figure 1 shows rotational population distributions of OH ($X^2\Pi$, $v=0$) for six different temperatures, ranging from 300 to 1800 K, based on simulations using LIFBASE [29]. As can be seen, the change in the shape of the population distributions between the lower temperatures (300, 600, and 900 K) is far greater than the change between the higher temperatures (1200, 1500, and 1800 K), suggesting higher sensitivity for OH thermometry at lower temperatures.

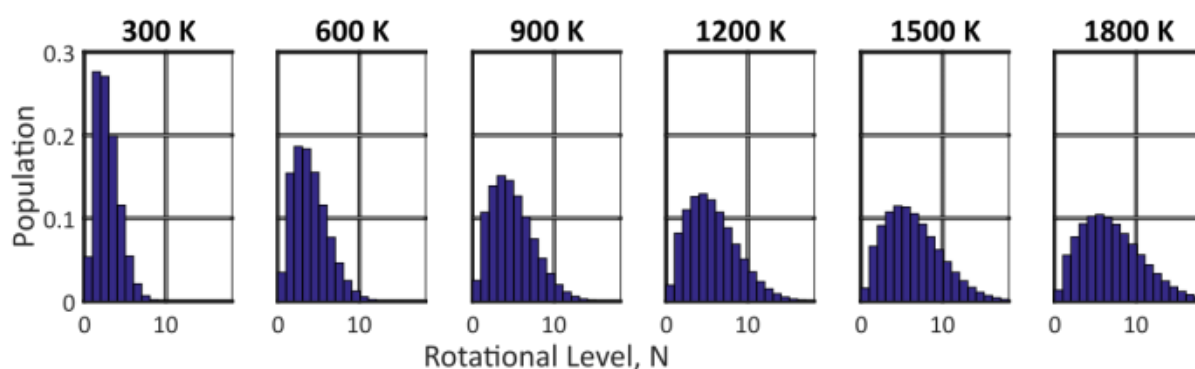


Fig. 1 Population distribution over rotational levels (N) in the vibrational band $v=0$ of OH ($X^2\Pi$) at six different temperatures ranging from 300 to 1800 K. The rotational levels are designated according to formalism corresponding to Hund's case b .

The OH radical is highly reactive and is present as an intermediate species in combustion reactions. Hence, the OH concentration is negligible before the temperature is high enough for these reactions to start. As an example, Fig. 2 displays simulated temperature and OH concentration profiles in a one-dimensional, stoichiometric methane/air flame. The flame was modeled using the Konnov detailed reaction mechanism [30] in the CHEMKIN-II collection of codes [31-33] including transport properties [34] from Sandia National Laboratories. As can be seen in the figure, the OH concentration is nearly zero for temperatures below 1000 K and the OH-LIF signal will thus drop rapidly with decreasing temperature. Due to the limited signal sensitivity and dynamic range of typical ICCD cameras, OH-based thermometry is typically limited to temperatures above 1000 K [35]. This fact constitutes a major drawback concerning

the use of OH radicals for combustion thermometry. Hence, in practice, it is not possible to probe the full probability distribution of temperatures in a combustion process using OH radicals as indicators. Additionally, temperatures cannot be extracted at temperatures where OH thermometry should be the most sensitive.

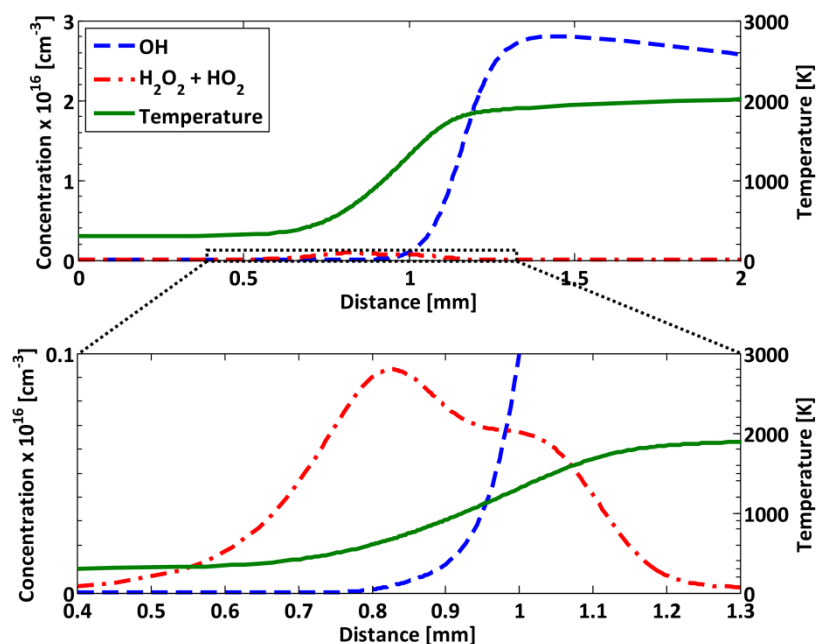


Fig. 2 OH concentration (blue dashed), $\text{H}_2\text{O}_2 + \text{HO}_2$ concentration (red dashed) and temperature (green line) profiles in a modeled one-dimensional methane/air flame at stoichiometric mixtures. The lower panel displays a closer view of the region marked with a dashed rectangle in the upper panel.

The lower panel of Fig. 2 clearly shows that there is a peak in the concentration of hydrogen peroxides at temperatures below 1000 K, where the OH concentration is virtually zero. Hence, the hydrogen peroxides may be utilized to acquire OH signal in this lower temperature range, where no OH signal ordinarily can be detected. With a sufficient photolysis irradiance, PFLIF can produce and probe OH fragments from H_2O_2 and HO_2 , as demonstrated in [25]. The basic principle of PFLIF is schematically illustrated for H_2O_2 in Fig. 3. A pump-laser pulse dissociates the parent molecules, i.e. H_2O_2 , into OH photofragments. A second laser pulse, tuned to an absorption line of OH, excites the OH photofragments whereupon the emitted

fluorescence is detected. Hydrogen peroxides (H_2O_2 and HO_2) are important intermediate species in various oxidation processes, e.g. combustion, plasma, and atmospheric chemistry [24]. Both molecules play a key role in low-temperature combustion chemistry, where it is well-known that the thermal decomposition of H_2O_2 into two OH fragments triggers auto-ignition in HCCI engines [36].

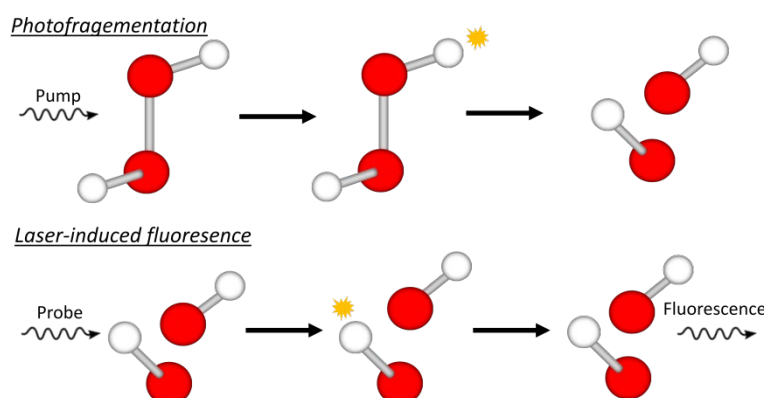


Fig. 3 The principle of PFLIF applied on hydrogen peroxide (H_2O_2). A pump laser excites the hydrogen peroxide molecule to a repulsive state and the molecule dissociates into two OH photofragments. A probe laser tuned to an absorption transition in OH excites the OH photofragments and the fluorescence emitted from these OH photofragments is proportional to the amount of hydrogen peroxide.

3. Experimental details

Temperatures were determined from OH excitation spectra recorded in three different temperature domains: 1) Room-temperature measurements carried out in a free flow of vaporized H_2O_2 . 2) Measurements at intermediate temperatures (400 - 600 K) at atmospheric pressure were performed in a preheating rig, containing a gaseous mixture of CH_4 , N_2 , O_2 , and O_3 . 3) High-temperature measurements at elevated pressures were undertaken in an operating optical HCCI engine. The reason for making the intermediate-temperature measurements in a preheated mixture of gaseous CH_4 , N_2 , O_2 , and O_3 (Experiment 2), and not in heated hydrogen peroxide is due to safety reasons, as heated hydrogen peroxide vapor represents a significant

hazard. Experiments 1) and 3) were carried out using laser sheets, allowing two-dimensional temperature imaging, while only averaged temperatures were extracted in experiment 2), which was performed with a mildly focused pump and an unfocused probe beam. Further details about the different measurement systems are given in the forthcoming sub-sections. The experimental setup was, however, similar for the three different studies and is schematically depicted in Fig. 4. Detailed information about the equipment used in the three experiments is given in Table 1.

The fourth-harmonic radiation at 266 nm from an Nd:YAG laser was used for photolysis. A frequency-doubled dye laser, operating with the dye Rhodamine 590, pumped by the second-harmonic radiation at 532 nm from an Nd:YAG laser, was used to probe the generated OH photofragments. The probe laser pulse must be delayed long enough to ensure that the OH photofragments have reached thermal equilibrium. Johansson et al. has shown that a time delay of 30 ns is long enough to thermalize OH photofragments stemming from 266-nm photolysis of H_2O_2 at room temperature and atmospheric pressure [24]. The pump and probe beams were first spatially overlapped using a dichroic mirror. The measurement volume was then intersected by the laser beams typically formed into vertical sheets using a cylindrical lens. The emitted OH fluorescence passed through an optical band-pass filter and was detected with an intensified CCD camera.

For the H_2O_2 vapor and preheating-rig experiments the tuning speed of the probe laser was 1 pm/s, i.e. it took 2000 s to record a 2-nm spectrum in these experiments. The camera acquires one frame per second, i.e. each image is an average of 10 (H_2O_2 vapor experiment, where the laser pulse repetition rate was 10 Hz) or 5 laser shots (preheating rig experiment, where the laser repetition rate was 5 Hz). The scans are thus based on 20000 or 10000 laser shots, respectively. For the engine measurements the probe laser had a tuning speed of 10 pm/s and, thus, it took 200 s to complete a scan. The camera recorded 10 images per second, i.e. one shot

per image, resulting in spectra based on 2000 laser shots. The spectral resolution was estimated to ~ 1 pm for all three experiments.

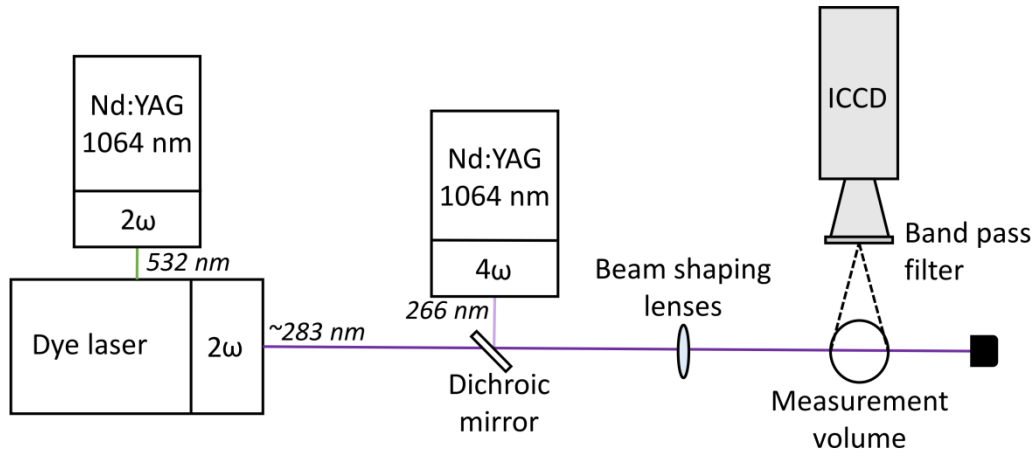


Fig. 4 Schematic illustration of the experimental setup used for OH-thermometry in the three different experiments.

Table 1 Major equipment used in the different experiments.

	Exp. 1, H ₂ O ₂ vapor	Exp. 2, Preheating rig	Exp. 3, HCCI engine
Pump laser (Nd:YAG)	Quantel, Brilliant-b	Ekspla, SL334	Quantel, Brilliant-b
Wavelength	266 nm	266 nm	266 nm
Pulse duration	5 ns	0.17 ns	5 ns
Rep. rate	10 Hz	5 Hz	10 Hz
Probe laser (dye laser)	Quantel, TDL90	Quantel, TDL90	Sirah, CSTR-G-2400
Pump laser	Quantel, YG981-E10	Quantel, YG981-E10	QuantaRay, PRO-250-10
Dye	Rh590	Rh590	Rh590
Linewidth	0.1 cm ⁻¹	0.1 cm ⁻¹	0.1 cm ⁻¹
Pulse duration	8 ns	8 ns	7 ns
Rep. rate	10 Hz	10 Hz	10 Hz
Scan speed in UV	1 pm/s	1 pm/s	10 pm/s
ICCD camera	Princ. Instr., PIMAX III	Princ. Instr., PIMAX III	Princ. Instr., PIMAX I
Number of pixels	1064×1064	1064×1064	512×512
Binning	4×4	4×4	2×8
Objective	f=100 mm, f/2 (B. Halle)	f=105 mm, f/4.5 (UV-Nikkor)	f=105 mm, f/4.5 (UV-Nikkor)
Beam focusing optics	Cyl. lens, f=300 mm (both beams)	Spher. lens, f=1 m (only pump beam)	Cyl. lens, f=200 mm (both beams)
Fluence in probe vol.	Pump: 30 mJ/mm ² Probe: 0.3 mJ/mm ²	Pump: 4 mJ/mm ² Probe: 0.002 mJ/mm ²	Pump: 32 mJ/mm ² Probe: 10 mJ/mm ²
Filters	WG305 (Schott) Band-pass: 307 ± 10nm	WG305 (Schott)	Bright line FF01-320/40- 25 (Semrock)

As can be seen in Table 1, the pump laser fluence is ~ 8 times higher in experiments 1 and 3 than in experiment 2. The reason for this is simply that high pump laser fluence was needed in these two experiments in order to obtain detectable concentrations of OH photofragments.

This is also the reason for the higher probe laser fluence employed in these measurements. In the experiments carried out in the preheating rig a good signal-to-noise ratio could be achieved with very low probe laser fluence, which is due to the high OH concentration produced in this case.

Temperature distributions have been extracted from OH-excitation spectra corresponding to the $A^2\Sigma^+ (v' = 1) - X^2\Pi (v' = 0)$ absorption band. The temperature evaluation was performed by fitting theoretical spectra of different temperatures to the experimental excitation spectra. Since the fluorescence signal was imaged onto a CCD camera, while scanning the probe laser wavelength, the recorded data contain an excitation spectrum in each group of binned pixels, allowing two-dimensional temperature images to be extracted. Such images were produced in experiments 1 and 3, where the laser beams were formed into thin sheets. The theoretical spectra were generated using LIFBASE [29] and convoluted with the instrument function of the experimental system. The instrument function was approximated by fitting theoretical spectra, at a reference temperature and pressure, to the experimental spectra. The theoretical spectra cover the wavelength interval 281.1 - 283.1 nm and correspond to excitation in the linear regime [29]. The fits were performed using a linear least-square algorithm.

3.1 H₂O₂ vapor

To verify the technique at room temperature, thermometry based on OH photofragments produced by photolysis of H₂O₂ vapor was carried out. The H₂O₂ vapor was generated by continuously bubbling nitrogen through a liquid 50:50 (wt-%) mixture of H₂O₂/H₂O contained in a bubbler flask at room temperature. Based on vapor pressure data for the mixture, the concentration of H₂O₂ in the vapor phase is estimated to 500 ppm. With the pump laser fluence given in Table 1, a photolysis quantum yield $\phi = 2$, and an absorption cross section $\sigma = 4.3 \cdot 10^{-20} \text{ cm}^2$ [37], the concentration of OH photofragments can be estimated to 150 ppm using

Equation (1) in [25]. The measurements were performed just above the opening of the bubbler flask. See reference [24] for further details about the measurement object and the experimental setup. The time delay between the pump and probe pulse was 1 μ s. This selection is not so critical since the chemistry consuming the created OH photofragments is rather slow, it takes about 50 μ s for the OH concentration to decay to the 1/e-point, and the OH concentration is essentially constant for pump-probe delays between 0-1 μ s [24]. It is, however, very important to use a delay that is long enough to ensure that the OH photofragments have reached thermal equilibrium, which is established within a few nanoseconds. The laser pulse energies were monitored by photo diodes and trended on an oscilloscope, allowing each image to be compensated for laser intensity variations in the post-processing of the recorded data.

3.2 Preheating gas rig

The preheating gas rig consists of three gas lines containing CH₄, O₂/O₃, and N₂, respectively, and these gases are mixed at the bottom of a 25-cm pipe with a diameter of 10 mm. Before the mixing process, N₂ is heated by a furnace and a thermocouple measures the temperature in the probe volume located 5 mm above the outlet. The rig was operated with a stoichiometric gas mixture of CH₄, O₂ and N₂, with a gas composition 0.33:1:4 l/min. The ozone flow was generated by an ozone generator providing 8400 ppm ozone at 470 K. During the PFLIF measurements, the O₃ molecules were dissociated into O(¹D) and O₂, whereupon the O(¹D) fragment reacts with mainly CH₄, producing OH and CH₃ radicals. The upper limit for the OH concentration in the measurement volume is estimated to 7600 ppm at 470 K. The photochemically produced OH radicals were detected by the probe laser, which was tuned across the same absorption band as previously described. Since the OH radicals are produced through photochemistry, the pump-probe delay should be long enough for a significant OH-concentration buildup. It was found that 1.5 μ s was an appropriate pump-probe delay, resulting

in an adequate signal-to-noise ratio. Excitation spectra at three different temperatures were recorded. The pulse energy of the probe laser was continuously monitored by a photodiode connected to an oscilloscope and this data was then used to perform background subtraction in each image and compensate for laser intensity fluctuation during the scan.

3.3 HCCI engine

Previously, our group has performed PFLIF in an HCCI engine to measure quantitative H_2O_2 concentrations [26, 27]. During that measurement campaign, excitation spectra were recorded on OH photofragments at two different piston positions in the compression stroke, namely at the crank angle degrees (CADs) -23 and -13, where 0 CAD corresponds to top dead center (TDC), i.e. the upper turning point of the piston. Using Equation (1) in [25] with the H_2O_2 mass fractions at -23 and -13 CAD reported in [26], i.e. 0.23% and 0.20%, the pump fluence given in Table 1, a photolysis quantum yield $\phi = 2$, and an absorption cross section $\sigma = 1.0 \cdot 10^{-19} \text{ cm}^2$ [38], the OH photofragment concentration is estimated to be roughly 0.1% at both crank angles. Due to the chemical consumption of the produced photofragments over time, a short time delay between the pump and probe pulse is desirable to generate high enough signal strength. At the same time it is important to have a long enough delay to ensure that the OH photofragments are thermal. Due to the elevated pressure at the two investigated CADs (15 and 22 bar), the time required to reach thermal equilibrium is significantly shorter than for atmospheric pressure. In our previous work the OH fragment signal intensity at -23 CAD has been measured at different pump-probe delay times and it was found that 20 ns is an appropriate delay [26]. A 20-ns pump-probe delay was therefore selected to maintain a high signal-to-noise ratio while still attaining thermal equilibrium and avoiding any prompt interference induced by the pump laser.

The test engine was a four-cylinder commercial D4D diesel engine manufactured by Toyota and modified for single-cylinder HCCI operation. To provide optical access, a quartz

cylinder ring and flat quartz piston was employed using a Bowditch extender. The fuel was a 50/50 mixture of the primary reference fuels iso-octane and n-heptane, i.e. PRF50, that was injected into the intake port to provide HCCI operation. Engine operating conditions and specifications are listed in Table 2. The engine was operated at 20 revolutions per second, the laser pulse repetition rate was 10 Hz (see Table 1), and the camera readout rate was 10 Hz, which implies that the ICCD camera recorded one image in each combustion cycle (every other cycle is combusting in a four-stroke engine).

Table 2 *Engine specifications*

Parameter	Value	Unit
Bore	82.2	mm
Stroke	94	mm
Connecting rod length	146	mm
Compression ratio	11.1:1	[-]
Engine speed	1200	RPM
Swirl ratio	2	[-]
Fuel equivalence ratio (ϕ)	0.26	[-]
Intake valve closing (IVC)	-149	CAD (after TDC)
Exhaust valve opening (EVO)	129	CAD (after TDC)

4. Results and discussion

4.1 Experiment 1 – Thermometry in vaporized hydrogen peroxide

Figure 5 shows an excitation spectrum recorded in vaporized H_2O_2 at room temperature and atmospheric pressure. The spectrum shown here was extracted by averaging the signal intensity in an area consisting of 50×120 superpixels (4×4) in the center of each image. Since such averaging may be performed in this case, as the temperature is assumed not to vary in the probe volume, we chose to show such a spectrum for clarity. The red curve at the top shows the difference between the experimental spectrum and the best-fit spectrum. As indicated by this residual curve, the best-fit spectrum generally agrees fairly well with the experimental spectrum. However, in particular, the measured peaks in the R_1 -branch, i.e. the peaks at the violet end of the spectrum (281.15 – 281.45 nm), are higher than the corresponding peaks in the fitted spectrum. There was of course a trade-off between adequate signal-to-noise ratio and ensured excitation in the linear regime, and the discrepancy suggests that the laser intensity might have been slightly too high, resulting in partial saturation. Furthermore, uncertainties in parameters describing the collisional broadening cause errors in the spectral line shapes of the theoretical spectrum, leading to deviations between the experimental and the fitted spectrum. Nevertheless, the result indicates that these deficiencies do not pose any significant error on the evaluated temperature (283 K).

In the determination of the two-dimensional temperature distribution no averaging was done – an excitation spectrum was extracted for each 4×4 -binned pixel. With laser sheets ~ 200 μm thick and the imaging optics employed (see Table 1), the spatial resolution is estimated to be $200 \times 100 \times 100$ μm^3 . The results are shown in Fig. 6, where the upper panel shows a color-coded temperature image and the lower panel displays the corresponding histogram of the temperature distribution. The histogram reveals a nearly Gaussian temperature distribution with a mean temperature of 283 K and a standard deviation of 12 K, i.e. 4.3% of the mean

temperature. Room temperature (295 K) is thus within the limit of uncertainty of the measurements. This result constitutes the precision and accuracy of the measurement technique at room temperature.

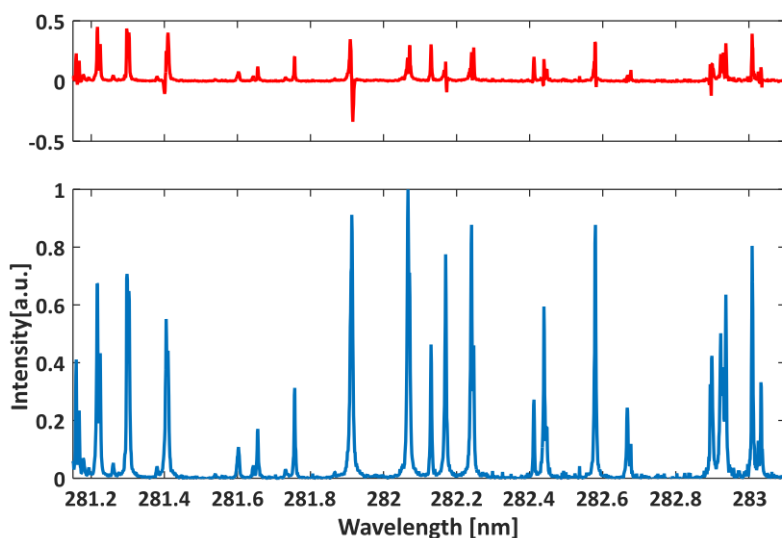


Fig. 5 Experimental excitation spectra of OH photofragments generated in hydrogen peroxide vapor at room temperature and pressure. The curve at the top is the difference between the experimental and best-fit spectrum. The evaluated temperature is 283 K.

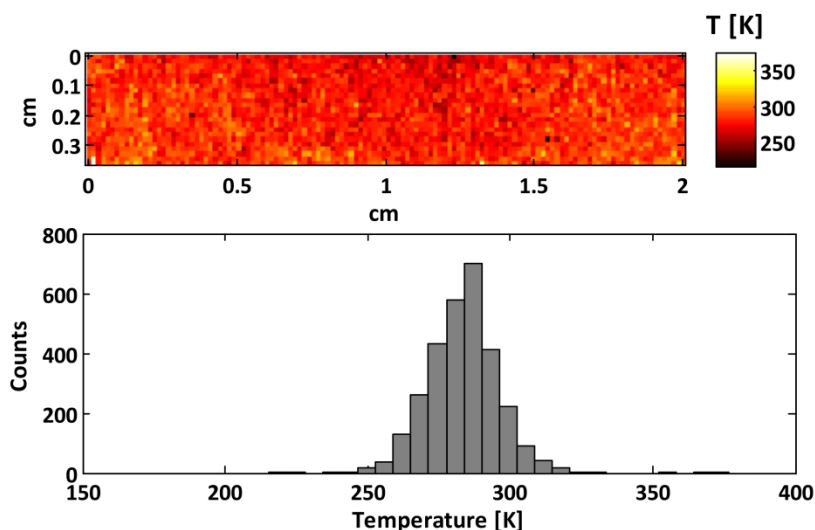


Fig. 6 Upper panel: Experimental OH 2-D temperature distribution in H_2O_2 vapor at ambient temperature and pressure. Lower panel: Histogram of the temperature distribution, where the mean temperature is 283 K with a standard deviation of 12 K (4.3%).

4.2 Experiment 2 – Thermometry in a preheated mixture of CH₄/N₂/O₂/O₃

Excitation spectra were recorded in a CH₄/N₂/O₂/O₃ mixture at three different levels of preheating, resulting in the temperatures 473, 516, and 559 K, measured by a thermocouple in the probe volume. The region containing strong OH signal, defined by the mildly focused pump laser beam (see Table 1), was averaged (20×60 superpixels) in the extraction of the excitation spectra. Averaging is justified as the temperature in the probe volume is assumed to be homogeneous. Figure 7 displays the excitation spectrum recorded at 516 K.

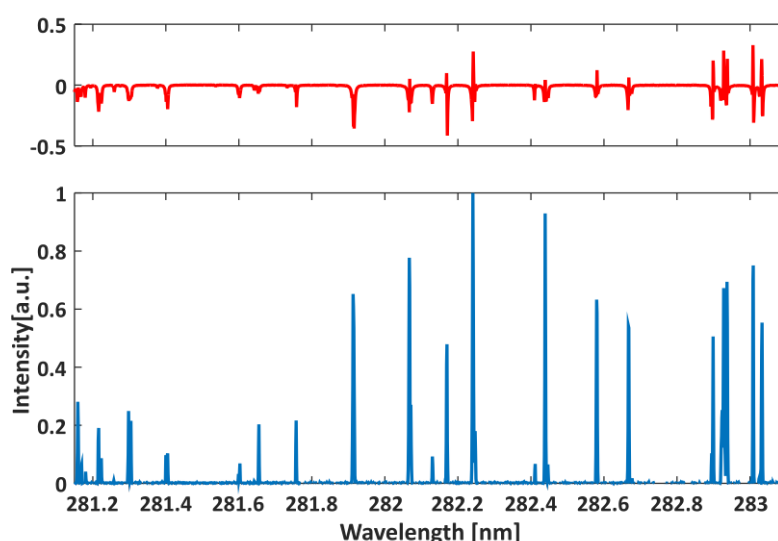


Fig. 7 Experimental excitation spectra of OH fragments generated in a preheated mixture of CH₄/N₂/O₂/O₃ at 516 K. The curve at the top is the difference between the experimental and best-fit spectrum. The evaluated temperature is 525 K.

In terms of relative peak heights, the residual curve indicates a generally good agreement between the measured and fitted spectrum. As can be seen the peaks are very narrow and their shapes exhibit virtually no Lorentz wings. In order to achieve good fits, the simulated spectra were generated assuming Doppler broadening and instrument broadening (pure Gaussian) as the only broadening mechanisms, i.e. no collisional broadening. The physical origin of this remarkable spectral feature has not been resolved by the authors. A closer look at the residual curve shows that there are deviations between the observed and fitted line shapes, suggesting

that a more advanced model for the spectral broadening is needed. It should be emphasized that the OH fragments detected in this case are resulting from 266-nm photolysis of O₃ into O(¹D) and O₂ (a ¹Δ_g) [39], followed by OH production through O(¹D) + CH₄ → OH + CH₃. In addition to this photochemistry, the heated mixture of CH₄/N₂/O₂/O₃ also results in low-temperature chemical reactions, wherefore the chemical composition surrounding the detected OH radicals is not known. Nevertheless, the present experiment was merely designed to generate OH radicals in an intermediate temperature regime, between room temperature and combustion temperatures, and as such it serves its purpose.

The results of the temperature evaluation are summarized in Table 3. The first column of the table presents the temperature in the probe volume measured with the thermocouple, the second column contains the temperatures evaluated from the excitation spectra, and in the third column the difference between the thermocouple temperature and the evaluated temperature is displayed. The evaluated temperatures correspond quite well with the temperatures measured with the thermocouple, especially for the two lower temperatures, for which the deviation is less than 2%. The larger deviation at the highest temperature might possibly be due to a larger impact of the aforementioned errors in the spectral lineshapes at this temperature.

Table 3 *Result of the measurements performed in a preheated mixture of CH₄/N₂/O₂/O₃.*

Thermocouple temperature [K]	OH temperature [K]	ΔT [K]
473	477	4
516	525	9
559	582	23

4.3 Experiment 3 – Thermometry in an HCCI engine

The third experiment represents an application of the thermometry concept in a practical combustion system, namely an HCCI-engine. Figure 8 shows an excitation spectrum corresponding to one 2×8 -binned pixel recorded at -23 CAD. The mean pressure at this piston position, i.e. 15 bar, extracted from measured pressure traces, was used as input data for calculation of the library of theoretical spectra. The mean pressure was also used to calculate a mean temperature, i.e. 816 K, using the ideal gas law. As can be seen in the figure, the peaks are much broader than in the two other cases (see Figs. 5 and 7), which is mainly a result of significant collisional broadening at the elevated pressure. The residual curve indicates a fairly good agreement between the measured and fitted spectrum. The fact that it is possible to obtain rather good fits indicates that cycle-to-cycle variations are not severe, which justifies the experiment as a proper demonstration of thermometry based on OH fragments, although we strongly recommend a technique with single-shot capacity for engine thermometry in general, which will be further discussed in Section 4.4.

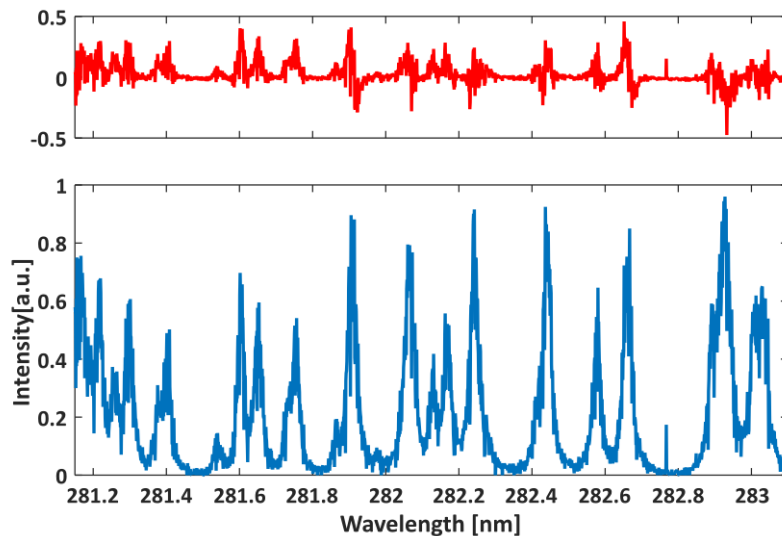


Fig. 8 *Excitation spectrum recorded in the HCCI engine at -23 CAD. The top panel shows the residual curve obtained by subtracting the best-fit theoretical spectrum from the experimental spectrum. The evaluated temperature is 860 K.*

The results of two-dimensional thermometry at -23 and -13 CAD are shown in Fig. 9. With laser sheets $\sim 150\text{ }\mu\text{m}$ thick, pixel binning 2×8 , and the imaging optics employed (see Table 1), the spatial resolution is estimated to be $150\times 50\times 200\text{ }\mu\text{m}^3$. Color-coded temperature images obtained at -23 and -13 CAD are shown in Fig. 9a and 9b, respectively, while the corresponding histograms of the temperature distributions are displayed in Fig. 9c and 9d, respectively. As can be seen in panels a and b, the height of the temperature image is smaller for -13 CAD than for -23 CAD, which is a consequence of the piston obstructing a part of the laser beam at -13 CAD. From the histogram shown in panel c it follows that the measured mean temperature at -23 CAD is 860 K, which agrees reasonably well with the mean temperature calculated from the measured pressure traces, i.e. 816 K. At -13 CAD, the mean pressure is 22 bar, and the histogram, shown in panel d, indicates a measured mean temperature of 1042 K, which is ~ 90 K higher than the 950 K calculated from the mean pressure. The fact that the measured temperature is higher than the calculated is however not surprising as the impact of low-temperature chemistry is not reflected in an ideal-gas-law calculation.

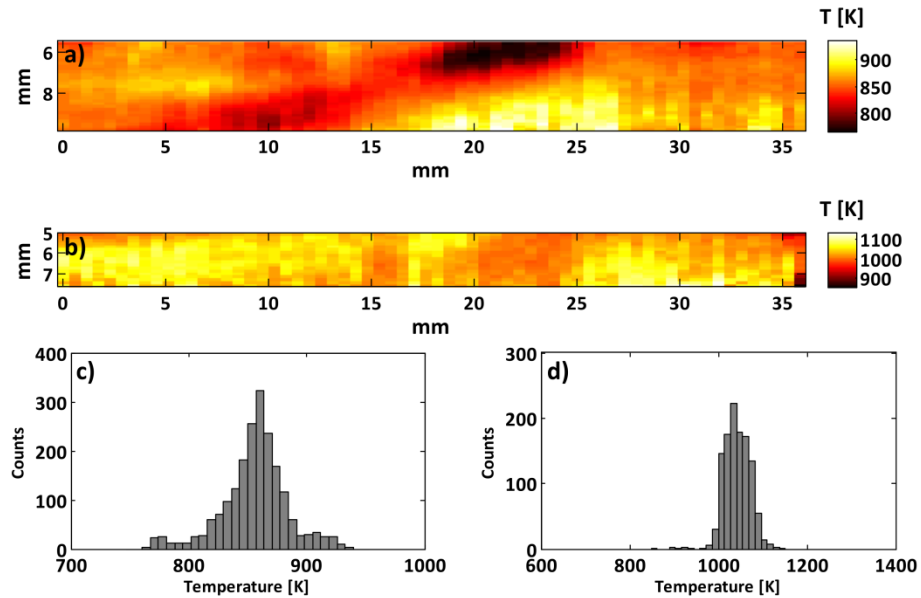


Fig. 9 Two-dimensional temperature maps determined from OH-excitation spectra recorded in the HCCI-engine at -23 CAD (a) and -13 CAD (b). The corresponding temperature histograms are shown

in panels (c) and (d). The mean temperatures are 856 K (-23 CAD) and 1042 K (-13 CAD), and the corresponding standard deviations are 28 K and 29 K, respectively.

As can be seen in the temperature images shown in Fig. 9, the temperature field is not perfectly uniform, but “islands” of low and high temperatures are present. Although, the quality of the spectral fits in general is quite good, errors caused by cycle-to-cycle variations are certainly induced to some extent. Regarding potential cycle-to-cycle variations in the concentration of H_2O_2 , i.e. the OH photofragment precursor, we have analyzed 100 single-shot images recorded at -23 CAD with the probe laser wavelength fixed at 282.93 nm. It was found that the relative standard deviation in the OH fluorescence signal is $\sim 15\%$, but since the signal is dependent on the product of the pump and probe laser intensities, whose relative standard deviations are $\sim 4\%$ (pump) and $\sim 8\%$ (probe), shot-to-shot fluctuations of the laser intensities constitute a significant part of the signal variation. In terms of cycle-to-cycle variations in the mean in-cylinder temperature caused by cycle-to-cycle variations in the mean pressure, these are estimated to be less than 1% as the relative standard deviations in the pressures measured at the two CADs are less than 1%. Another source of uncertainty is the fact that relatively high probe laser intensities were employed in order to obtain adequate signal-to-noise ratio, which means that the recorded OH excitation spectra correspond to partially saturated fluorescence, while the fitted spectra corresponds to excitation in the linear regime. The fact that the degree of saturation varies across the probe volume may induce spatial variations in the resulting temperature maps. Therefore, we refrain from drawing any quantitative conclusions regarding the observed inhomogeneities in the temperature fields. However, we note that inhomogeneities in both concentration and temperature distributions in HCCI engines have been observed previously [40].

4.4 Further development of the concept

Thermometry based on excitation spectra was chosen in order to clearly demonstrate the new concept based on OH photofragments. The major limitation of this approach is that it does not allow single-shot measurements. Instead, the obtained data are averaged over time. In the engine application the spectra are recorded during 200 s, i.e. 2000 combustion cycles, which results in temperature distributions that do not reflect potential cycle-to-cycle variations.

To further develop the technique, to provide instantaneous imaging capacity, a two-line excitation concept could be utilized. Temperature would then be extracted from the ratio between fluorescence signals generated through excitation from two rotational levels whose population ratio is highly temperature dependent. Such a concept can be realized with essentially the same setup and equipment as employed in the present studies, except that two probe laser beams, tuned to two different rovibronic transitions, are required. The ratio between the two fluorescence signals generated carries temperature information, which can be extracted quantitatively through calibration measurements. Optimum selection of the two transitions for OH excitation will depend on the conditions prevailing in the probe volume. Devillers et al. thoroughly investigated various strategies for optimized two-line OH LIF thermometry in engines [23]. With the method proposed in this work, realized with 2-line probing of OH, instantaneous 2-D thermometry in engines can be carried out over a significantly wider range of crank-angle degrees than with the methods currently available. Thus, thermometry would be possible both in the cool-flame regime, prior to ignition, and in the high-temperature regime after ignition. Moreover, studies of thermal boundary layers close to surfaces are possible. Such measurements are paramount for the understanding of heat transfer between the gas and cylinder walls, knowledge that is required in order to maximize the efficiency of combustion engines. It should, however, be noted that even with a 2-line concept, allowing single-shot recordings, temperature determination is only possible in regions where OH is present, either

as photofragments or naturally occurring. Thus, if the probed volume is inhomogeneous, extraction of mean temperatures is precarious as the sampling will be biased if there are locations where OH is not present.

In terms of extending the technique to other combustion engine concepts and other fuels it is difficult to make a general assessment of the potential as the concentration of hydrogen peroxides is strongly dependent on the local temperature, i.e. it is dependent on both the fuel and the combustion mode. In our experiment performed in an HCCI engine operating with the fuel PRF50 the H_2O_2 concentration is relatively high ($\sim 0.2\%$). For HCCI combustion, simulations show similar H_2O_2 concentration levels for pure n-heptane [41] and for natural gas [42]. A simulation based on the same engine as the one used in the present experiments but operated in Diesel mode with pure n-heptane, suggests that the peak hydrogen peroxide concentration is an order of magnitude lower under these conditions as compared to the concentration in the present engine. The simulation, performed with the software Digital analysis of reaction systems (DARS), was based on small skeletal kinetics model coupled to a stochastic reactor model as described in [26]. A general assessment of the potential for thermometry based on OH photofragments originating from hydrogen peroxides obviously requires a detailed analysis of the low-temperature chemistry for different fuels and various engine combustion modes. Nevertheless, our estimates for a few different cases suggest that the method seems to be better suited for HCCI engines than for Diesel engines.

5. Conclusions

In this work, we have shown that photolytically/photochemically produced OH can be used for thermometry, and expand the temperature range of OH fluorescence thermometry in an HCCI engine. By producing OH photofragments from precursor molecules, such as H_2O_2 , present in

a low-temperature regime, OH fluorescence can be obtained at temperatures where the natural OH radical concentration is negligible. Another important asset that the concept brings is improved accuracy and precision due to the stronger temperature dependence of the OH rotational population distribution at lower temperatures. In addition to a tunable laser for OH excitation (probe laser), a pulsed UV laser is needed for photolysis (pump laser); here a frequency-quadrupled Nd:YAG laser (266 nm) was employed. Temperatures are determined from OH excitation spectra, recorded by scanning the probe laser wavelength across the $A^2\Sigma^+(v=1) - X^2\Pi(v=0)$ absorption band (around 282 nm), to which simulated spectra are fitted. The probe laser pulse must be delayed long enough to ensure that the OH photofragments have reached thermal equilibrium, 10 ns being long enough for most applications at atmospheric or higher pressures.

The technique is successfully demonstrated for 1-D and 2-D thermometry in three different temperature regimes; at room temperature, using UV photolysis of vaporized H_2O_2 for generation of OH photofragments, at intermediate temperatures (470 – 560 K), using UV photolysis of O_3 , which produces an oxygen atom that reacts with CH_4 , whereupon OH is formed, and at elevated temperatures (860 – 1040) and pressures (15 - 22 bar), through measurements in an optical HCCI engine, where OH photofragments are formed through UV photolysis of H_2O_2 and HO_2 , which are present prior to ignition. Overall the accuracy is found to be better than 5%, with the major error source being partial saturation of the OH fluorescence. The precision in terms of the standard deviation of the temperatures evaluated in each pixel of the 2-D image recorded at room temperature was found to be 12 K, i.e. 4%.

In order to achieve instantaneous imaging capacity, we plan to replace the scanning with a two-line OH excitation scheme. Temperature would then be extracted from the ratio between fluorescence signals generated through excitation from two rotational levels whose population ratio is highly temperature dependent. Such a concept can be realized with essentially the same

setup and equipment as employed in the present studies, except that two probe laser beams, tuned to two different rovibronic transitions, are required. We believe that such a measurement tool, allowing for example in-cylinder studies of cycle-to-cycle variations in the 2-D temperature field, would be of significant value in engine research, as it can deliver experimental data for validation of combustion models in a broad temperature range.

Acknowledgement

The authors would like to thank Martin Algotsson, Martin Tunér and Bengt Johansson for running and financing the HCCI-engine, and Bo Li and Zhongshan Li for the laser diagnostic measurements in the HCCI-engine. The present work has been financed by DALDECS, an Advanced Grant from the European Research Council (ERC), and by Centre for Combustion Science and Technology (CECOST) through the Swedish Energy Agency (Energimyndigheten) and the Swedish Foundation for Strategic Research (SSF).

References

- [1] S.R. Turns, An introduction to Combustion: Concepts and Applications, The McGraw-Hill Companies, 2001.
- [2] C. Copeland, J. Friedman, M. Renksizbulut, Planar temperature imaging using thermally assisted laser induced fluorescence of OH in a methane–air flame, *Exp. Therm. Fluid Sci.* 31 (2007) 221-236.
- [3] S. Roy, J.R. Gord, A.K. Patnaik, Recent advances in coherent anti-Stokes Raman scattering spectroscopy: Fundamental developments and applications in reacting flows, *Prog. Energy Combust. Sci.* 36 (2010) 280-306.
- [4] A. Bohlin, C.J. Kliewer, Diagnostic Imaging in Flames with Instantaneous Planar Coherent Raman Spectroscopy, *J. Phys. Chem. Lett.* 5 (2014) 1243-1248.
- [5] A.C. Eckbreth, Laser diagnostics for combustion temperature and species, Gordon and Breach Publishers, Amsterdam, Netherlands, 1996.
- [6] M. Aldén, P. Grafstrom, H. Lundberg, S. Svanberg, Spatially resolved temperature measurements in a flame using laser-excited two-line atomic fluorescence and diode-array detection, *Opt. Lett.* 8 (1983) 241-243.

- [7] J. Nygren, J. Engström, J. Walewski, C. Kaminski, M. Aldén, Applications and evaluation of two-line atomic LIF thermometry in sooting combustion environments, *Meas. Sci. Technol.* 12 (2001) 1294.
- [8] K. Kohse-Höinghaus, R.S. Barlow, M. Aldén, J. Wolfrum, Combustion at the focus: laser diagnostics and control, *Proc. Combust. Inst.* 30 (2005) 89-123.
- [9] M. Aldén, J. Bood, Z. Li, M. Richter, Visualization and understanding of combustion processes using spatially and temporally resolved laser diagnostic techniques, *Proc. Combust. Inst.* 33 (2011) 69-97.
- [10] K. Kohse-Höinghaus, Laser techniques for the quantitative detection of reactive intermediates in combustion systems, *Prog. Energy Combust. Sci.* 20 (1994) 203-279.
- [11] H.P. Broida, Rotational Temperatures of OH in Methane-Air Flames, *J. Chem. Phys.* 19 (1951) 1383-1390.
- [12] J.H. Bechtel, R.E. Teets, Hydroxyl and its concentration profile in methane-air flames, *Appl. Opt.* 18 (1979) 4138-4144.
- [13] C. Chan, J.W. Daily, Measurement of temperature in flames using laser induced fluorescence spectroscopy of OH, *Appl. Opt.* 19 (1980) 1963-1968.
- [14] K.J. Rensberger, J.B. Jeffries, R.A. Copeland, K. Kohse-Höinghaus, M.L. Wise, D.R. Crosley, Laser-induced fluorescence determination of temperatures in low pressure flames, *Appl. Opt.* 28 (1989) 3556-3566.
- [15] B. Atakan, J. Heinze, U.E. Meier, OH laser-induced fluorescence at high pressures: spectroscopic and two-dimensional measurements exciting the A–X (1,0) transition, *Appl. Phys. B* 64 (1997) 585-591.
- [16] K. Hayashida, K. Amagai, M. Arai, LIF thermometry in sooty flames using NO $D^2\Sigma^+ \leftarrow X^2\Pi(0,1)$ and OH $A^2\Sigma^+ \leftarrow X^2\Pi(3,0)$ bands, *Energy* 30 (2005) 497-508.
- [17] J. Kiefer, A. Meyerhoefer, T. Seeger, A. Leipertz, Z.S. Li, M. Aldén, OH-thermometry using laser polarization spectroscopy and laser-induced fluorescence spectroscopy in the OH A-X (1,0) band, *J. Raman Spectrosc.* 40 (2009) 828-835.
- [18] R.P. Lucht, N.M. Laurendeau, D.W. Sweeney, Temperature measurement by two-line laser-saturated OH fluorescence in flames, *Appl. Opt.* 21 (1982) 3729-3735.
- [19] R. Cattolica, OH rotational temperature from two-line laser-excited fluorescence, *Appl. Opt.* 20 (1981) 1156-1166.
- [20] J.M. Seitzman, R.K. Hanson, P.A. DeBarber, C.F. Hess, Application of quantitative two-line OH planar laser-induced fluorescence for temporally resolved planar thermometry in reacting flows, *Appl. Opt.* 33 (1994) 4000-4012.
- [21] R. Giezendanner-Thoben, U. Meier, W. Meier, M. Aigner, Phase-locked temperature measurements by two-line OH PLIF thermometry of a self-excited combustion instability in a gas turbine model combustor, *Flow Turbul. Combust.* 75 (2005) 317-333.
- [22] D.R. Crosley, G.P. Smith, Vibrational energy transfer in laser-excited $A^2\Sigma^+$ OH as a flame thermometer, *Appl. Opt.* 19 (1980) 517-520.
- [23] R. Devillers, G. Bruneaux, C. Schulz, Development of a two-line OH-laser-induced fluorescence thermometry diagnostics strategy for gas-phase temperature measurements in engines, *Appl. Opt.* 47 (2008) 5871-5885.
- [24] O. Johansson, J. Bood, M. Aldén, U. Lindblad, Detection of hydrogen peroxide using photofragmentation laser-induced fluorescence, *Appl. Spectrosc.* 62 (2008) 66-72.
- [25] O. Johansson, J. Bood, B. Li, A. Ehn, Z.S. Li, Z.W. Sun, M. Jonsson, A.A. Konnov, M. Aldén, Photofragmentation laser-induced fluorescence imaging in premixed flames, *Combust. Flame* 158 (2011) 1908-1919.
- [26] B. Li, M. Jonsson, M. Algotsson, J. Bood, Z.S. Li, O. Johansson, M. Aldén, M. Tunér, B. Johansson, Quantitative detection of hydrogen peroxide in an HCCI engine using photofragmentation laser-induced fluorescence, *Proc. Combust. Inst.* 34 (2013) 3573-3581.

- [27] G. Coskun, M. Jonsson, J. Bood, M. Tunér, M. Algotsson, B. Li, Z. Li, H.S. Soyhan, M. Aldén, B. Johansson, Analysis of in-cylinder H_2O_2 and HO_2 distributions in an HCCI engine – Comparison of laser-diagnostic results with CFD and SRM simulations, *Combust. Flame* 162 (2015) 3131-3139.
- [28] J. Bood, P.-E. Bengtsson, F. Mauss, K. Burgdorf, I. Denbratt, Knock in spark-ignition engines: end-gas temperature measurements using rotational CARS and detailed kinetic calculations of the autoignition process, SAE Technical Paper 0148-7191, 1997.
- [29] J. Luque, D.R. Crosley, LIFBASE: Database and Spectral Simulation Program (Version 1.6), SRI International Report MP 99-009 (1999).
- [30] A.A. Konnov, Implementation of the NCN pathway of prompt-NO formation in the detailed reaction mechanism, *Combust. Flame* 156 (2009) 2093-2105.
- [31] R.J. Kee, J.F. Grcar, M.D. Smoke, J.A. Miller, Sandia National Laboratories Report, SAND86-8240, 1990.
- [32] R.J. Kee, F.M. Rupley, J.A. Miller, Sandia National Laboratories Report, SAND89-8009, 1990.
- [33] A.E. Lutz, R.J. Kee, J.A. Miller, Sandia National Laboratories Report, SAND87-8248, 1990.
- [34] R.J. Kee, G. Dixon-Lewis, J. Warnatz, M.E. Coltrin, J.A. Miller, Sandia National Laboratories Report, SAND86-8246, 1990.
- [35] U.E. Meier, D. Wolff-Gaßmann, W. Stricker, LIF imaging and 2D temperature mapping in a model combustor at elevated pressure, *Aerosp. Sci. Technol.* 4 (2000) 403-414.
- [36] S. Tanaka, F. Ayala, J.C. Keck, A reduced chemical kinetic model for HCCI combustion of primary reference fuels in a rapid compression machine, *Combust. Flame* 133 (2003) 467-481.
- [37] J. Nicovich, P. Wine, Temperature-dependent absorption cross sections for hydrogen peroxide vapor, *J. Geophys. Res. Atmos.* 93 (1988) 2417-2421.
- [38] D. Baulch, R. Cox, R. Hampson Jr, J.A. Kerr, J. Troe, R. Watson, Evaluated kinetic and photochemical data for atmospheric chemistry, *J. Phys. Chem. Ref. Data* 9 (1980) 295-472.
- [39] R. Schinke, G.C. McBane, Photodissociation of ozone in the Hartley band: Potential energy surfaces, nonadiabatic couplings, and singlet/triplet branching ratio, *J Chem. Phys.* 132 (2010) 044305.
- [40] R. Yu, X.-S. Bai, A. Vressner, A. Hultqvist, B. Johansson, J. Olofsson, H. Seyfried, J. Sjöholm, M. Richter, M. Aldén, Effect of turbulence on HCCI combustion, SAE Technical Paper No. 2007-01-0183, 2007.
- [41] R. Hasegawa, I. Sakata, T. Koyama, H. Yanagihara, Numerical analysis of ignition control in HCCI engine, SAE Technical Paper No. 0148-7191, 2003.
- [42] S.M. Aceves, D.L. Flowers, C.K. Westbrook, J.R. Smith, W. Pitz, R. Dibble, M. Christensen, B. Johansson, A multi-zone model for prediction of HCCI combustion and emissions, SAE Technical paper No. 0148-7191, 2000.